Korean J. Chem. Eng., 36(7), 1201-1207 (2019)
DOI: 10.1007/s11814-019-0300-4

pISSN: 0256-1115
eISSN: 1975-7220

Development of an advanced hybrid process coupling TiO_2 photocatalysis and zeolite-based adsorption for water and wastewater treatment

Min Kwang Kim*, Seo-Hyun Pak, Min Chang Shin*, Chan-gyu Park**, Edoardo Magnone*, and Jung Hoon Park*,†**

*Dongguk University, Wonheung-gwan F619, 30, Pildong-ro 1gil, Jung-gu, Seoul 04620, Korea
**Environmental Technology Division, Korea Testing Laboratory, 87, Digital-ro 26-gil, Guro-gu, Seoul 08389, Korea
(*Received 16 March 2019 • accepted 15 May 2019*)

Abstract−We present an advanced hybrid process coupling a fixed-bed photocatalysis reactor with the TiO_2 photocatalyst film coated on microstructured α-Al_2O_3 hollow fibers (AlHF) under UV exposure, with a second fixed-bed reactor where the zeolite-based adsorbent is fixed onto AlHF support for water and wastewater treatment. The physicochemical properties of both coated films were investigated by X-ray diffraction (XRD), Brunauer-Emmett-Teller (BET) method, scanning electron microscopy (SEM), and energy dispersive X-ray (EDX). The sequential activity of the dual fixed bed reactor was overall evaluated by examining the degradation of 20 ppm Methylene Blue (MB), 1 ppm Iron and 0.04 ppm Arsenic solution as a general model of a complex aqueous solution containing not only an organic pollutant but also heavy metal and toxic cations. The results show that the proposed hybrid process by coupling two processes together could remove MB, Fe (II), and As (III) effectively, and the removal rates reached nearly 90%, 30%, and 70%, respectively, in 1 hour. These excellent results using the UV-TiO_2/zeolite-based adsorbent combined process could be attributed to a synergistic effect between photocatalysis and adsorption process.

Keywords: TiO_2, Hollow Fiber, Decomposition, Zeolite, Tetraethyl Orthosilicate

INTRODUCTION

The importance of water resources, as well as their sustainable use, treatment, and purification, are all priorities that need to be addressed to ensure that our water will be protected for future generations. Due to this importance, extensive researches have conducted on the purification of water and wastewater treatment. In particular, during the past two decades, increasing attention has been paid to TiO_2 photocatalysts due to their high photocatalytic properties regarding organic compounds, low cost, and non-toxicity as well as high chemical stability [1]. When the TiO_2 is irritated with UV light having energy above the band gap of 3.2 eV, an electron is excited from the valence band into the conduction band and excited electrons and holes are generated. The excited electrons and holes move to the surface of the photocatalyst. The excited electrons form superoxide radical ions (O_2-), and the holes left in the valence band can form reactive hydroxyl radical (OH). The radicals contribute to photocatalytic oxidation reaction [2-4]. When powder photocatalyst was used, there are some problems of difficulty of recovery after the reaction and low photoactivity due to the agglomeration of powder and light scattering. The solution of these problems is based on utilization and development of a photocatalyst immobilized on appropriate support for heterogeneous catalytic removal of toxic substances and organic compounds. Many researchers have tried to explore the various possibilities by different coating techniques, like sputtering [5-7], sol-gel [8-10], and chemical vapor deposition [11-14].

In our previous works, α-Al_2O_3 hollow fibers (AlHF)-supported TiO_2 photocatalysts were prepared by a single dip-coating process by the help of an adhesion promoter as a silica-based binder (SBB) for the effective photodegradation of the Methylene Blue (MB) under UV irradiation [15]. From our previous work, the best performance was achieved with an SBB AlHF-supported TiO_2 photocatalysts, whereby a degradation ratio of about 65% was obtained [15].

In the field of water treatment technologies to remove contaminants and undesirable components, it is also important to reduce heavy metal concentration. In particular, heavy metals are toxic and do not biodegrade, so they have a profound effect on all living things [16]. The heavy metal ions contained in water can be removed by various methods such as ion exchange, precipitation, and adsorption. In this study, heavy metal ions were removed by using a zeolite capable of selectively adsorbing specific ions. However, the pores of the zeolite are generally too small and the diffusion rate of water is very slow [17]. The mesoporous zeolite adsorbent accelerates the diffusion rate of the reactants, facilitates access to active sites where heavy metal ions are adsorbed, and increases the specific surface area, which is advantageous for heavy metal adsorption removal. The mesoporous zeolite adsorbent was prepared by a recrystallization process in which the framework was broken and was recrystallized [18]. Also, in the case of mesoporous zeolite adsorbent in powder form, as in the above case of TiO_2 photocatalyst powers, it is difficult to separate adsorbate-mesoporous zeolite mixture from the aqueous solution after adsorption. Recent reports in the literature have suggested that this problem can be resolved by the immobilization of mesoporous zeolite on a support so that it not only can

†To whom correspondence should be addressed.
E-mail: pjhoon@dongguk.edu

effectively separate adsorbent from wastewater, but also improve the removal rate of heavy metals [19,20]. Recently, Huang et al. reported the layer-by-layer synthesis of sandwich-like zeolite Linde Type A (LTA) membranes by using 3-aminopropyltriethoxysilane (APTES) as covalent linkers between the zeolite layer and the porous Al_2O_3 support [21].

In the field of water and wastewater treatment, our research aims at finding a solution to this challenging problem of purification of water by the simultaneous reduction of the organic pollutants and toxic heavy metals. The aim of this work is to develop an advanced hybrid process coupling a fixed-bed photocatalysis reactor with the TiO_2 film coated on the microstructured AlHF under UV exposure, with a second fixed-bed reactor where the zeolite-based adsorbent is fixed onto AlHF support. As far as we know, no previous research has investigated the sequential activity of a dual bed reactor system that includes a first reactor where the UV irradiation is used to break down organic compounds in a photodegradation process followed by a second reactor operating in series containing AlHF-supported zeolite-based adsorbents to reduce the heavy metal concentration by an adsorption process. The experiments were performed with an aqueous solution of MB (20 ppm), Fe (1 ppm), and As (0.04 ppm) as a solution model containing not only an organic pollutant but also heavy metal and toxic cations [22-26]. The removal performance of the overall hybrid process was studied and presented.

EXPERIMENT

1. Microstructured α-Al_2O_3 Hollow Fiber (AlHF)

Microstructured α-Al_2O_3 hollow fibers (AlHF) were fabricated by a phase inversion process as reported in Ref. [27]. In detail, dope solution consists of 60 wt% Al_2O_3 powder (Alumina, 99.9%, Kceracell, Korea), 33.5 wt% 1-methyl-2-pyrrolidinone (NMP, 99.5%, Samchun Pure Chemical Co. Ltd., Korea), 6 wt% polyethersulfone (PESf, Ultrason® E6020P, BASF, Germany), and 0.5 wt% polyvinyl-pyrrolidone (PVP, Sigma Aldrich, USA). The solution was stirred for 12 h at room temperature and degassed by a vacuum pump (IDP3, Varian, U.S.A.) for 60 minutes. After this time, the AlHFs were prepared by a spinning process with an extrusion pressure of one bar and an air gap of 10 cm. Deionized water was used for the phase inversion process as internal and external coagulant. The AlHFs were dried at 100 °C for 24 hours and calcined at 1,300 °C for 4 hours.

2. AlHF-supported TiO_2 Photocatalysts

The TiO_2 powders were prepared using tetrabutyl orthotitanate (TBOT, 97%, Sigma Aldrich, USA) as a precursor by the sol-gel method. In detail, 15 mL of TBOT and an aqueous solution (100 mL) of nitric acid (1.5 mL) were mixed. The solution was stirred for 30 minutes by magnetic stirrers at room temperature. After, 30 mL of iso-propanol (IPA, >99.0%, Samchun Pure Chemical Co. Ltd., Korea) was added to the solution and stirred again for 180 minutes. Finally, the mixture was dried at 100 °C for one night and then calcined at 400 °C for 210 minutes.

The obtained TiO_2 powder was coated on the surface of 3 cm AlHFs by a dip coating method. A coating solution of 12.5 wt% TiO_2 powder in 80 wt% ethanol (99.9%, Samchun Pure Chemical Co. Ltd., Korea) and 7.5 wt% silica-based binder solution was used. The silica-based binder was prepared using tetraethyl orthosilicate (TEOS, 98%, Sigma Aldrich, USA). For additional details see Ref. [28]. Fig. 1 is a flowchart diagram showing the preparation of TiO_2 powders and AlHF-supported TiO_2 photocatalysts.

3. AlHF-supported Zeolite-based Adsorbents

The AlHF-supported mesoporous zeolite Y was coated by a meso-Y sol on the NH_2-functionalized AlHF supports as reported in Ref. [21]. NaOH solution (0.2 M) was mixed with 0.18 M of commercial zeolite Y (H-type, Si/Al≈30). The obtained solution was stirred at 35 °C for 1 h to obtain a viscous solution called mesoporous Y sol. The amount of 40 mL of prepared mesoporous Y sol was poured into a Teflon-lined stainless steel autoclave (50 mL) with the NH_2-functionalized AlHF supports (2 gr., length=3 cm). The resultant mixture was heated at 145 °C in an oven for 24 h. The resulting AlHF-supported zeolite-based adsorbents were washed

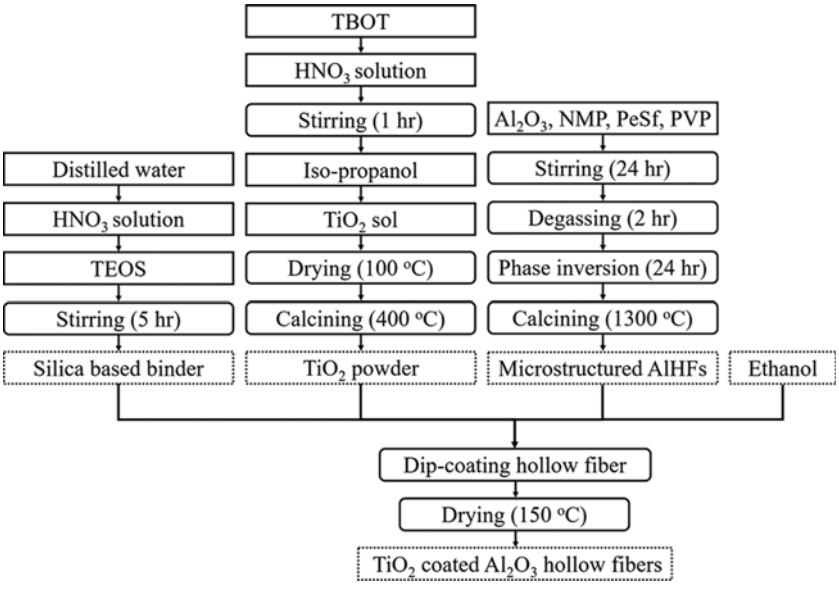

Fig. 1. Flowchart diagram of the synthesis of TiO_2 powders, and fabrication of α-Al_2O_3 hollow fibers and TiO_2 coated hollow fiber photocatalyst.

with ethanol and then calcined at 550 °C for 2 h. Finally, AlHF-supported zeolite-based adsorbents were added to a 100-mL aqueous solution of 10% $FeCl_3$ (≥99.99%, Sigma Aldrich) and mixed for 60 min at 90 °C. The water was removed using a vacuum distiller and the remaining AlHF-supported zeolite-based adsorbent was dried in two steps: room temperature for 2 h and 250 °C for 2 h.

4. Characterization

Non-coated AlHF, AlHF-supported TiO_2 photocatalysts, and AlHF-supported zeolite-based adsorbents were characterized by means of scanning electron microscopy (FE-SEM, S-4800, Hitachi, Japan) and energy dispersive spectrometer (EDS, S-4800, Hitachi, Japan). The crystal structure and phase composition were analyzed by X-ray diffraction (XRD, Ultima IV, Rigaku, U.S.A.) spectrum at room temperature with CuKα radiation (λ=1.542 Å) within the 2θ range from 20-80°.

The prepared samples were analyzed for its Brunauer-Emmett-Teller (BET) surface area and BET pore size distribution. N_2 adsorption desorption isotherms were measured at a bath temperature of −195.85 °C by a Micromeritics Tristar 3000 instrument. Prior to analyzing the sample, it was degassed for at least 10 hours. The value of BET specific surface area was calculated using a software Tristar 3000. In addition, pore size distribution area and volume were estimated by applying T-method micropore analysis.

5. Testing of Photocatalytic Activity and Adsorbent Capacity

The activity of the dual fixed bed reactor was overall evaluated by examining the rate degradation of a mixture of organic pollutant, heavy metal, and toxic cations in water. A solution of 20 ppm MB, 1 ppm Iron and 0.04 ppm Arsenic in water (500 mL) was used for the experiments. The pollutant solution was supplied at a flow rate of 100 mL/min using a gear pump (Gear Pump, REGLO-Z Digital, ISMATEC, U.S.A.). A schematic view of the hybrid dual fixed bed reactor plant coupling TiO_2 photocatalytic decompositions and zeolite-based adsorptions for water and wastewater treatment is shown in Fig. 2. Removal percentage of MB, As, Fe was determined by:

$$\text{(MB, As, Fe) Removal (\%)} = \frac{C_0 - C_t}{C_0} \times 100$$

Regarding the first fixed-bed photocatalysis reactor with the TiO_2 photocatalyst film coated on the microstructured α-Al_2O_3 hollow fibers, four UV-LED lamps (8W UV, Osram, Germany) were positioned vertically at the border of the cylindrical quartz reactor and the main wavelength of the UV lamp is 254 nm (Relative strength= 90.0%). 15 g of AlHF-supported TiO_2 photocatalysts was loaded into photocatalysis reactor. Regarding the second fixed-bed reactor where the zeolite-based adsorbent is fixed onto Al_2O_3 hollow fiber support, the same amount of AlHF-supported zeolite-based adsorbents (15 gr) was used.

A sample of the solution was taken after the second reactor every 15 minutes and the amount of remaining MB was analyzed by a UV-visible spectrometer (UV-vis, Optizen Pop, Mecasys, Korea). The UV-visible spectrometer was calibrated with 5, 10, 15, and 20 ppm standard samples of MB aqueous solutions as reported in Ref. [15]. The concentration of As and Fe was determined by ICP Atomic Emission Spectrometer (Inductively Coupled Plasma, 730ES, Australia) using standard recommended methods (Mn: Periodate Oxidation Method Fe : FerroVer® Method).

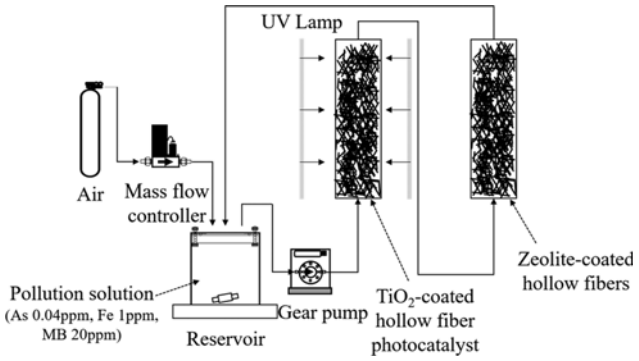

Fig. 2. Hybrid process reactors coupling TiO_2 photocatalysis and zeolite-based adsorptions for water and wastewater treatment.

RESULTS AND DISCUSSION

The crystal structure and phase composition of TiO_2 photocatalytic powders and AlHF-supported TiO_2 photocatalysts were estimated by X-ray diffraction. Fig. 3 shows the XRD patterns of the prepared TiO_2 photocatalytic powders and AlHF-supported TiO_2 photocatalysts as well as the Joint Committee on Powder Diffraction Standards (JCPDS) cards No. 10-173, No. 21-1272, and No. 21-1276 for comparison purposes with Al_2O_3, anatase and rutile TiO_2 phases, respectively. From XRD pattern of prepared TiO_2 powder, anatase and rutile phases were both detected. This result suggests that the TiO_2 powder is a mixture of anatase and rutile phases. In detail, the XRD peak intensity of the anatase phase (80%) TiO_2 was much stronger than rutile (20%) phase TiO_2. As expected for a TiO_2 thin-film deposited on the surface of AlHF supports the ob-

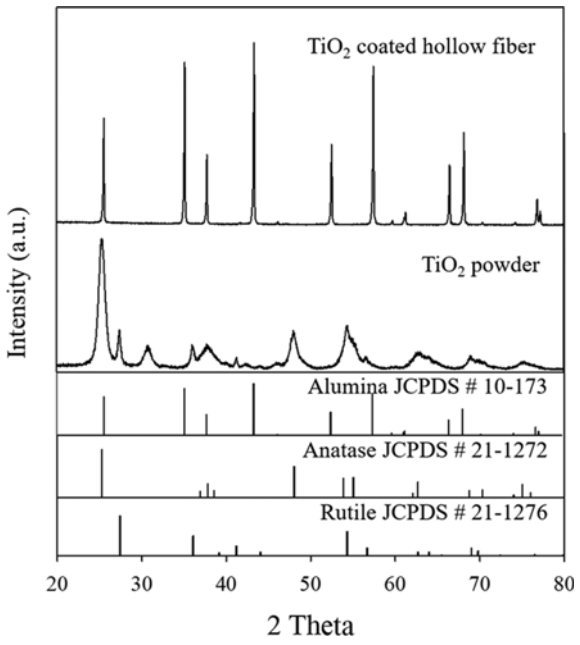

Fig. 3. XRD result of TiO_2 powder prepared by sol-gel method and TiO_2 coated hollow fibers.

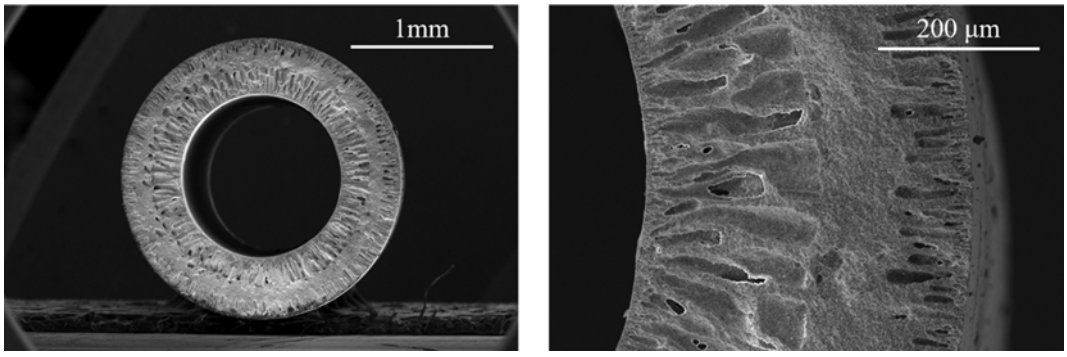

Fig. 4. SEM Images of the cross section of non-coated AlHF.

tained XRD patterns are difficult to interpret because TiO_2 phases are present at, or near, detection limits of XRD. Thus as expected, the XRD pattern of the TiO_2 coated hollow fiber is dominated by Al_2O_3 reflections within the detection limit of XRD measurement. Also, the XRD peaks of the prepared TiO_2 powders are broad with a large full width half maximum, and this can indicate the formation of TiO_2 nanocrystallites. This is consistent with what has been found in previous research concerning the adhesion strength of TiO_2 photocatalytic powders on the surface of microstructured AlHFs through the use of an adhesion promoter [15].

Fig. 4 shows the SEM images of the cross section of microstructure AlHF prepared by a phase inversion process before the coating process. The external and internal surface of α-Al_2O_3 hollow fiber has a finger-like pore structure, and the middle area between the external and internal surface has a sponge-like pore structure. The pore of the internal surface was larger than the internal surface. A similar pattern of results regarding the pore structure of AlHF was obtained in Ref. [27].

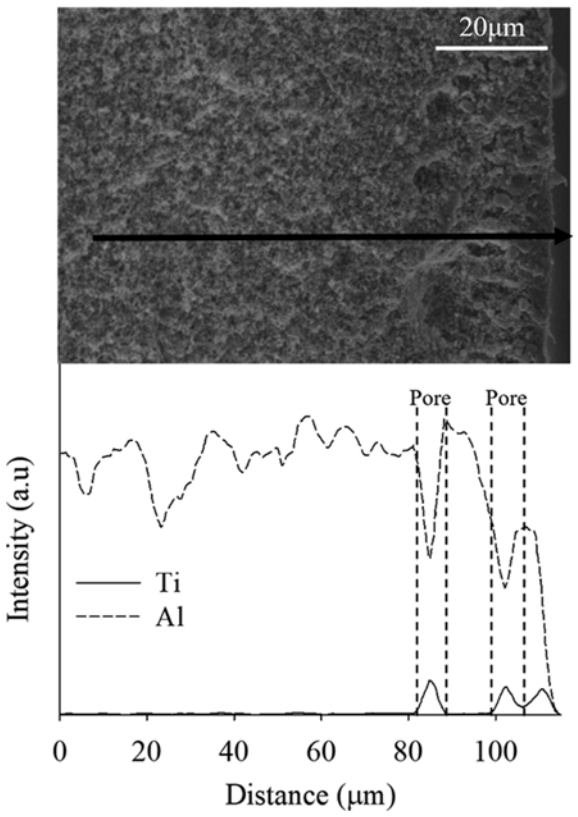

Fig. 5. EDS line scanning result of the cross section of AlHF-supported TiO_2 photocatalysts.

In detail, Fig. 5 exhibits the external cross section of AlHF-supported TiO_2 photocatalysts. The recorded EDS line scan of the cross section reveals that the average TiO_2 film thickness was about 8 μm as measured with the surface profile. Note that the TiO_2 probably was coated not only on the AlHF surface but also inside its pores. In fact, this hypothesis is also supported by the appearance of two broad peaks at 10-20 and 30-40 μm deep under AlHF surface regarding titanium, and it happened to correspond with a minimum of aluminum.

Fig. 6 shows the EDS elemental distribution maps of Al and Ti at the surface of AlHF-supported TiO_2 photocatalysts. The TiO_2 particle has a high degree of dispersion and uniform distribution on the AlHF surface. The results are directly in line with previous findings where a good distribution of nanosized TiO_2 photocatalysts on the surfaces of AlHF-TiO_2 is achieved by using an adhesion promoter to increase the adhesion strength between TiO_2 and AlHFs [15].

Fig. 7 shows the elemental distribution of silica - the main constituent atom of the zeolite - of the AlHF-supported zeolite-based adsorbents. The elemental mapping image indicated that Si was distributed along the inner diameter of AlHF. It is hypothesized that this distribution regarding the zeolite-based adsorbent to the inside wall of the AlHF can help the adsorption not only of the decomposition products derived from first fixed-bed photocatalysis reactor with the TiO_2 photocatalyst film coated on the AlHF under UV exposure but also the heavy metal and toxic cations like iron and arsenic, as studied in this work.

The N_2 adsorption/desorption isotherm of the non-coated AlHF and AlHF-supported zeolite-based adsorbents were analyzed by BET technique and the results are represented in Fig. 8(a). In the case of AlHF-supported zeolite-based adsorbents, the shape of obtained curves, called type I isotherms, is typical of microporous solids where only monolayer adsorption occurs [29]. It is interesting that the BET surface area of the coated-AlHF zeolite-based adsorbent was found to be about 32.11 m^2/gr, which is almost eight-times bigger than the previous non-coated AlHF (4.11 m^2/g). The BET surface areas obtained in this work for the AlHF-supported zeolite-

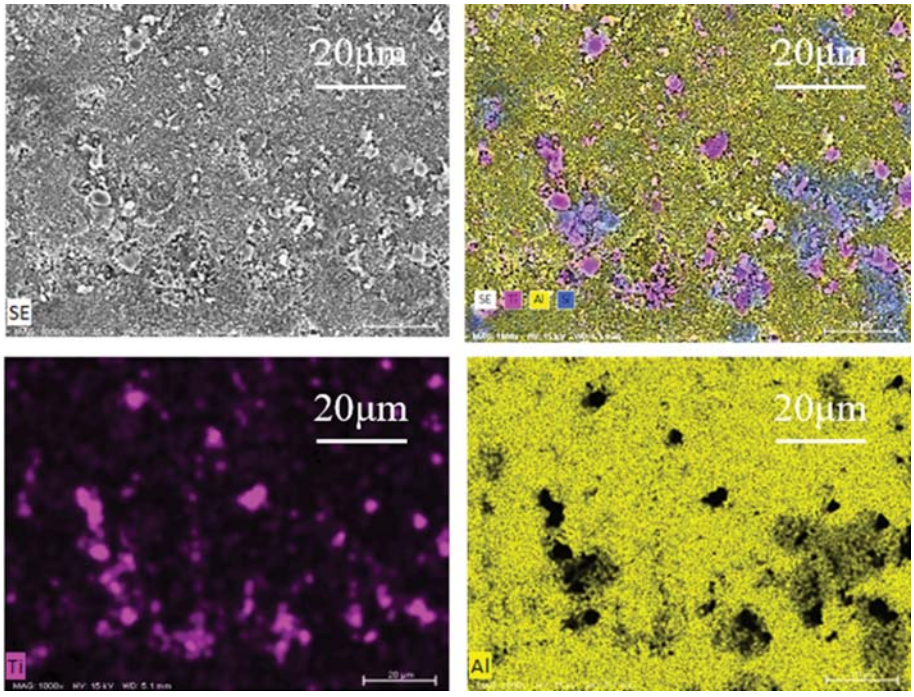

Fig. 6. SEM image and elemental distribution of titanium and alumina on the surface of AlHF-supported TiO_2 photocatalysts.

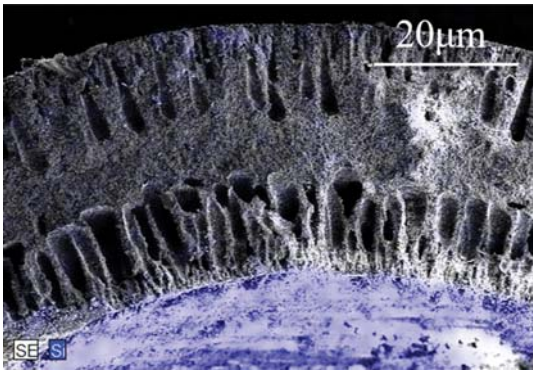

Fig. 7. Elemental distribution of silica on the cross section and surface of AlHF-supported zeolite-based adsorbents.

based adsorbents are comparable with that reported by Simsek et al. [30]. This result suggested that the AlHF surface modification procedure by zeolite-based adsorbent powders was effective on the final BET surface characteristics of samples [31]. This result is confirmed by the data presented in Fig. 8(b), which illustrates the BET pore size distribution plots for the non-coated AlHF and AlHF-supported zeolite-based adsorbent samples based on N_2 adsorption/desorption isotherm. As can be seen from Fig. 8(b), the differences in pore size distribution among before and after zeolite-based adsorbent coating process were mainly in the region where pore width was smaller than 4 nm. Regarding the pore size, Fig. 8(b) also suggests that there is a great difference between original AlHFs and the samples where the zeolite-based adsorbent is fixed onto Al_2O_3 hollow fiber support. The curve of the pore diameter distribution for AlHF-supported zeolite-based adsorbent has prominent peaks in

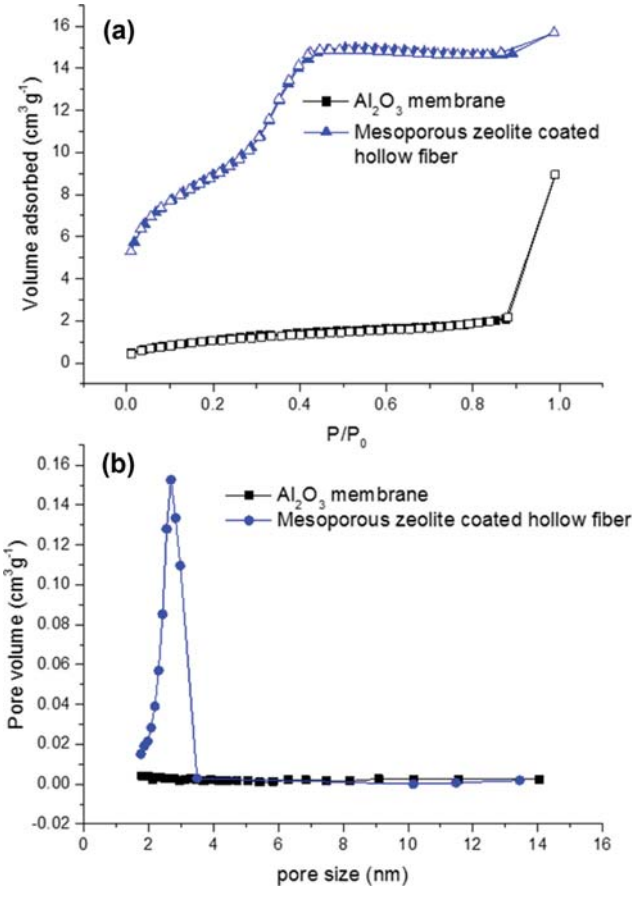

Fig. 8. (a) Nitrogen adsorption-desorption isotherms and (b) pore size distribution of non-coated AlHF and AlHF-supported zeolite-based adsorbents.

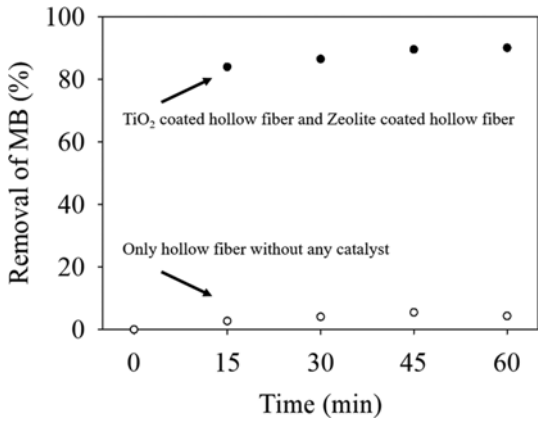

Fig. 9. Photocatalytic decomposition of the MB under UV light using hybrid processes coupling TiO_2 photocatalysis and zeolite-based adsorption for water and wastewater treatment.

the regions of 2-4 Å, corresponding to about the micropore region. This is an indication of the formation of highly microporous zeolite-based adsorbent with a narrow pore width distribution for the AlHF-supported zeolite-based adsorbent sample in comparison with non-coated AlHF. In addition, the t-method micropore analysis was used to know the micropore volume of AlHF-supported zeolite-based adsorbents [32]. The micropore area for non-coated AlHF and AlHF-supported zeolite-based adsorbent are 2.91 and 31.78 cm^3/g, respectively. From these results, it is clear that the zeolite-based adsorbents strongly modified the surface of AlHF. The pore size of AlHF-supported zeolite-based adsorbents is an important parameter in the adsorption process as it may be one of the principal factors that determines the overall hybrid processes coupling TiO_2 photocatalysis and zeolite-based adsorptions process.

Fig. 9 shows the result of the decomposition of MB by a hybrid processes coupling TiO_2 photocatalysis and zeolite-based adsorptions for water and wastewater treatment. The ratio decomposition of MB was achieved at about 84% after just 15 minutes and about 90% after 60 minutes. In our previous work, we evaluated TiO_2-coated AlHF used to remove MB under UV light irradiation and in the same conditions of the present work without the second fixed-bed reactor with zeolite-based adsorbent fixed onto AlHF support [15]. As reported in the previous work [15], with a single fixed-bed photocatalysis reactor based on a TiO_2 photocatalyst film coated on the AlHF, the MB ratio decomposition was achieved about 35%, 55%, and 65%, after 10, 30, and 60 minutes, respectively. Instead, when the hybrid processes coupling TiO_2 photocatalysis and zeolite-based adsorptions were used, the MB decomposition rate was faster than the single TiO_2 photocatalysis process. At this point, we decided to investigate also the single contribution of AlHFs on the overall process by a new experiment with only non-coated AlHFs under the same previous conditions. In this case, the MB ratio decomposition was reached at 4% after 60 minutes (see Fig. 9). This result provides evidence for the existence of a synergistic effect between photocatalysis and adsorption process that is not dependent on AlHF support.

The treatment and purification towards Fe (II) and As (III) in the hybrid process were also studied. Table 1 shows the summary

Table 1. Removal of iron and arsenic using a hybrid process coupling TiO_2 photocatalysis and zeolite-based adsorption

	Only hollow fiber without any catalyst	TiO_2 coated hollow fiber and zeolite coated hollow fiber
Fe	0.95	0.783
As	0.023	0.013

results for the purification of a solution of 20 ppm Methylene Blue (MB), 1 ppm Iron and 0.04 ppm Arsenic with non-coated AlHFs and a hybrid processes coupling TiO_2 photocatalysis and zeolite-based adsorptions supported AlHFs. In the first case, the concentration of Fe (II) changed from 1 to 0.95 mg/L with an iron removal percentage of −5% after 60 minutes. At the same time, the As (III) concentration decreased from 0.04 to 0.023 mg/L with a removal efficiency of −42.5%. Instead, when the experiment was conducted by a hybrid processes coupling TiO_2 photocatalysis and zeolite-based adsorptions, the Fe (II) and As (III) removal ratios were about −22% and −69%, respectively. Taken together, the present findings suggest that there is a kind of synergism that evolves when a TiO_2 photocatalyst reactor for the decomposition of an organic pollutant (MB) works in series with a second fixed-bed reactor where the zeolite-based adsorbent can adsorb heavy metal (Fe) and toxic cations (As).

CONCLUSIONS

An advanced hybrid process coupling a fixed-bed photocatalysis reactor with the TiO_2 photocatalyst film coated on the AlHF surface under UV exposure, with a second fixed-bed reactor, where the zeolite-based adsorbent is fixed onto AlHF support for water and wastewater treatment, was presented. The hybrid processes coupling TiO_2 photocatalysis and zeolite-based adsorption supported AlHFs were successfully used to simultaneously decrease the presence of organic pollutant (MB), heavy metal (Fe) and toxic cations (As).

In summary, there is a synergic effect between the TiO_2 photocatalytic decompositions and zeolite-based adsorptions. In detail, the MB, Fe and As removal efficiencies of −90%, −22%, and −68%, respectively, were obtained after 60 minutes of work. A blank test was performed using only AlHF without any catalysts or absorbers, and removal of MB, Fe, and As reached −4%, −5%, and −42.5%, respectively. The contributions made here have wide applicability in the field of water and wastewater treatment.

ACKNOWLEDGEMENTS

This research was supported by a grant (18CTAP-C133297-02) from Technology Advancement Research Program (TARP) funded by Ministry of Land, Infrastructure and Transport of Korean government.

REFERENCES

1. K. Hashimoto, H. Irie and A. Fujishima, *Jpn. J. Appl. Phys.*, **44**, 8269 (2005).
2. C.-H. Wu and J.-M. Chern, *Ind. Eng. Chem. Res.*, **45**, 6450 (2006).

3. H. J. Lee, Y. G. Park, S. H. Lee and J. H. Park, *Korean Chem. Eng. Res.*, **56**, 156 (2018).
4. S. H. Kim, S. G. Jeong, S. E. Na, S. Y. Kim and C. S. Ju, *Korean Chem. Eng. Res.*, **51**, 195 (2013).
5. S.-H. Jeong, J.-K. Kim, B.-S. Kim, S.-H. Shim and B.-T. Lee, *Vacuum*, **76**, 507 (2004).
6. P. Löbl, M. Huppertz and D. Mergel, *Thin Solid Films*, **251**, 72 (1994).
7. M. Yamagishi, S. Kuriki, P. Song and Y. Shigesato, *Thin Solid Films*, **442**, 227 (2003).
8. S.-Y. Lien, D.-S. Wuu, W.-C. Yeh and J.-C. Liu, *Sol. Energy Mater. Sol. Cells*, **90**, 2710 (2006).
9. C. Guillard, B. Beaugiraud, C. Dutriez, J.-M. Herrmann, H. Jaffrezic, N. Jaffrezic-Renault and M. Lacroix, *Appl. Catal. B*, **39**, 331 (2002).
10. J. Y. Hur, H. I. Lee, Y. K. Park, O. S. Joo, G. N. Bae and J. M. Kim, *Korean Chem. Eng. Res.*, **44**, 399 (2006).
11. X. Zhang and L. Lei, *Appl. Surf. Sci.*, **254**, 2406 (2008).
12. Z. Ding, X. Hu, P. L. Yue, G. Q. Lu and P. F. Greenfield, *Catal. Today*, **68**, 173 (2001).
13. D. Byun, Y. Jin, B. Kim, J. K. Lee and D. Park, *J. Hazard. Mater.*, **73**, 199 (2000).
14. S. C. Jung, S. C. Kim and S. G. Seo, *Korean Chem. Eng. Res.*, **39**, 385 (2001).
15. E. Magnone, M.-K. Kim, H. J. Lee and J. H. Park, *Ceram. Int.*, **45**, 3359 (2019).
16. A. El-Bayaa, N. Badawy and E. A. AlKhalik, *J, Hazard. Mater.*, **170**, 1204 (2009).
17. S.-H. Park, S.-M. Park, J. An and C.-g. Park, *Desalination Water Treat.*, **123**, 150 (2018).
18. W.-y. Shi, H.-b. Shao, H. Li, M.-a. Shao and S. Du, *J. Hazard. Mater.*, **170**, 1 (2009).
19. K. Sadowska, K. Góra-Marek and J. Datka, *J. Phys. Chem. C.*, **117**, 9237 (2013).
20. C.-C. Chang, A. R. Teixeira, C. Li, P. J. Dauenhauer and W. Fan, *Langmuir*, **29**, 13943 (2013).
21. A. Huang, N. Wang and J. Caro, *Micropor. Mesopor. Mater.*, **164**, 294 (2012).
22. L. Lu, Y. Zhang, P. Xiao, X. Zhang and Y. Yang, *Environ. Eng. Sci.*, **27**, 281 (2010).
23. C. Xu, G. Rangaiah and X. Zhao, *Ind. Eng. Chem. Res.*, **53**, 14641 (2014).
24. W. Yu, X. Liu, L. Pan, J. Li, J. Liu, J. Zhang, P. Li, C. Chen and Z. Sun, *Appl. Surf. Sci.*, **319**, 107 (2014).
25. R. S. Dariania, A. Esmaeili, A. Mortezaali and S. Dehghanpour, *Optik*, **127**, 7143 (2016).
26. H. Taghvaei, M. Farhadian, N. Davari and S. Maazi, *Adv. Environ. Technol.*, **4**, 205 (2017).
27. E. Magnone, H. J. Lee, J. W. Che and J. H. Park, *J. Ind. Eng. Chem.*, **42**, 19 (2016).
28. S. W. Kim, M. Kang and S. J. Choung, *J. Ind. Eng. Chem.*, **11**, 416 (2005).
29. S. M. Manocha, *Sadhana*, **28**, 335 (2003).
30. E. B. Simsek, E. Özdemir and U. Beker, *Chem. Eng. J.*, **220**, 402 (2013).
31. D. Mohan and C. U. Pittman Jr., *J. Hazard. Mater.*, **142**, 1 (2007).
32. N. Setoyama, T. Suzuki and K. Kaneko, *Carbon*, **36**, 1459 (1998).